Evolution of inflation-generated magnetic field through phase transitions

Tina Kahniashvili,[1,2,3,*] Axel Brandenburg,[4,5,†] Leonardo Campanelli,[6,‡] Bharat Ratra,[7,§] and Alexander G. Tevzadze[8,‖]

[1]*Department of Physics and The McWilliams Center for Cosmology, Carnegie Mellon University, 5000 Forbes Ave, Pittsburgh, Pennsylvania 15213, USA*

[2]*Department of Physics, Laurentian University, Ramsey Lake Road, Sudbury, Ontario P3E 2C, Canada*

[3]*Abastumani Astrophysical Observatory, Ilia State University, 3-5 Cholokashvili Avenue, Tbilisi GE-0194, Georgia*

[4]*Nordita, KTH Royal Institute of Technology and Stockholm University, Roslagstullsbacken 23, 10691 Stockholm, Sweden*

[5]*Department of Astronomy, AlbaNova University Center, Stockholm University, 10691 Stockholm, Sweden*

[6]*Dipartimento di Fisica, Università di Bari, I-70126 Bari, Italy*

[7]*Department of Physics, Kansas State University, 116 Cardwell Hall, Manhattan, Kansas 66506, USA*

[8]*Faculty of Exact and Natural Sciences, Tbilisi State University, 1 Chavchavadze Avenue, Tbilisi 0128, Georgia*

(Received 25 June 2012; published 7 November 2012)

We study the evolution of an inflation-generated magnetic field, due to its coupling to fluid motions, during cosmological phase transitions. We find that the magnetic field stays almost unchanged on large scales, while on small scales, the spectrum is modified in such a way that power at small scales becomes progressively suppressed. We also show that the magnetic field generates turbulent motions in the initially turbulence-free plasma. On large scales, the slope of the resulting kinetic energy spectrum is consistent with that of white noise.

DOI: 10.1103/PhysRevD.86.103005 PACS numbers: 98.70.Vc, 98.80.−k

I. INTRODUCTION

The origin of the coherent large-scale (~ 10 kpc) part of galactic magnetic fields, of μG strength, is under active discussion [1–4]. On larger, Mpc scales, until recently, there were only upper limits, the most restrictive being of order a few nG depending on the observational technique used to measure the intergalactic magnetic field strength [5]. Recently, there have been a number of published lower limits on a putative large-scale magnetic field of strength $10^{-1\pm1}$ fG(1 fG $= 10^{-15}$ G) [6], or possibly two orders of magnitude smaller [7].[1]

Almost certainly, the galactic fields are the amplified remnants of significantly weaker "seed" magnetic fields. Quantum mechanical fluctuations during inflation [9] is a leading candidate for generating the needed seed magnetic field [10–12]. To generate a large enough seed magnetic field through quantum mechanical fluctuations during inflation, conformal invariance must be broken during inflation. A simple, realistic, illustrative model couples the Abelian vector field with field strength tensor $F_{\mu\nu}$ to the scalar inflaton field ϕ through a dilatonlike coupling, generalizing the Maxwell Lagrangian density to $e^{\alpha\phi}F_{\mu\nu}F^{\mu\nu}$ where α is a parameter [11,12]. In the case of power-law inflation, and depending on the value of α, this can result in a large enough seed magnetic field to explain the observed galactic magnetic fields. This is an observationally viable model. For a more detailed description of the model, see Sec. II below.

After the end of inflation, such an inflation-generated magnetic field will be correlated over super-Hubble-radius scales. It would induce observable signatures in the cosmic microwave background (CMB) radiation anisotropies at the epoch of recombination (the last scattering surface) if its current amplitude on Mpc scales is of the order of a nG [13].[2] The properties of an inflation-generated primordial seed magnetic field depend on the parameters of the inflation model. If cosmological observations confirm the presence of an inflation-generated magnetic field, these measurements could be used to probe the physical conditions during inflation, including the shape of the inflaton potential energy density as well as the coupling between the inflaton and the vector gauge field.

To check the consistency of the model, the primordial magnetic field shape and amplitude should be measured in as many ways as possible. The simplest limit arises from the cosmological expansion dynamics during big bang nucleosynthesis. This requires that the energy density of the magnetic field should not be larger than about 10% of the radiation energy density. This limits the present (inflation-generated) magnetic field strength to less than a few μG, if the primordial magnetic field were generated prior to or during big bang nucleosynthesis, and was

*tinatin@phys.ksu.edu
†brandenb@nordita.org
‡Leonardo.Campanelli@ba.infn.it
§ratra@phys.ksu.edu
‖aleko@tevza.org

[1]These techniques for limiting a large-scale cosmological magnetic field might be unreliable [8], but see their Sec. IV where they note that more work will be needed to firm up these arguments and to determine whether the techniques used to establish the lower limits are indeed unreliable.

[2]The effects of an homogeneous magnetic field on the CMB anisotropy, and the resulting non-Gaussianity, are discussed in Ref. [14].

not damped or amplified by a magnetohydrodynamic (MHD) or some other process and so stays frozen into the plasma [15].

In addition to the CMB temperature anisotropies which a primordial magnetic field induces (as mentioned above), such a field will Faraday-rotate the CMB polarization anisotropies [16]. Currently available Faraday rotation data give a bound on the primordial magnetic field strength of less than a few nG (for a scale-invariant or homogeneous primordial magnetic field).

Another interesting signature of a cosmological magnetic field is the relic gravitational wave signal generated by the anisotropic magnetic stress [17]. The amplitude of the induced gravitational waves is determined by the magnetic field energy density, so a direct measurement of the resulting gravitational wave signal can lead to an independent limit on the magnetic field strength; see Ref. [18] and references therein.

After the Universe reheats at the end of inflation, the plasma which was created then has large conductivity, and it is conventional to assume that this remains the case as the Universe evolves to the present. In this case, the large-scale cosmological magnetic field behaves as a frozen-in field with an evolution determined by the simple, flux-conservation, dilution of magnetic field lines, $\mathbf{B}(\mathbf{x}, t) \propto \mathbf{B_0}(\mathbf{x})/a^2(t)$, where t is the physical cosmic time and $a(t)$ is the cosmological scale factor. On the other hand, the evolution of a primordial magnetic field is a complex process influenced by MHD as well as by the dynamics of the Universe [19–22]. In particular, the presence of a magnetic field can dramatically affect primordial turbulence (e.g., when the turbulence is associated with cosmological phase transition bubble motions) [19,23,24]. Furthermore, the presence of a magnetic field itself might lead to the development of turbulent motions, and so affect the turbulence [25,26].

In a recent examination [27] of the effects of the MHD coupling between a primordial magnetic field and turbulence during a cosmological phase transition, we considered two different initial shapes for the spectrum of the primordial magnetic field: a single-scale magnetic field and a magnetic field with a Batchelor spectrum at large scales. In this paper, we present a similar analysis for modified initial conditions for an inflation-generated primordial magnetic field [11], coupled via the usual MHD equations with the fluid, during the electroweak or QCD phase transitions. We consider both nonhelical and helical magnetic field cases.

We assume that the phase transition bubbles induce a typical length scale at which the magnetic field starts to interact with the phase transition fluid. The relevant difference between the electroweak and QCD phase transitions is encoded in the difference between values of parameters such as the temperature $T_\star$, the number of relativistic degrees of freedom $g_\star$, the bubble number, and bubble sizes. We assume initial absence of primordial turbulence, i.e., we assume that the plasma is initially at rest (although it is possible to generate turbulent motions through bubble collisions and nucleation [28]). The characteristic parameter of the primordial magnetic field is the root-mean-square (rms) Alfvén velocity $v_A = B/\sqrt{16\pi\rho_{\rm rad}/3}$. Here, $\rho_{\rm rad} \simeq \rho_{\rm thermal}$ is the radiation energy density. We use $\Omega_{\rm rad}h_0^2 = 2.56 \times 10^{-5}$, where $\Omega_{\rm rad}$ is the radiation energy density parameter and h_0 is the Hubble constant in units of $100\ {\rm km\,s^{-1}\,Mpc^{-1}}$, for a current CMB temperature $T_0 = 2.74$ K. At temperature $T_\star$, $\rho_{\rm rad}(T_\star) = \pi^2 g_*(T_*)^4/30$. The Alfvén velocity does not depend on $T_\star$ but is weakly dependent on $g_\star$, i.e., $v_A \propto g_\star^{-1/6}$.

In our previous simulations [27], we studied phase-transition-generated magnetic fields coupled to a relativistic fluid and discovered that equipartition between kinetic and magnetic energy densities is reached within reasonably short times. In this paper, our main purpose is to consider different initial conditions. In particular, in the case when the magnetic field is generated during inflation, we investigate the kinds of turbulent motions which result from the coupling of the magnetic field with the fluid, and determine how this affects the evolution of the field itself. We show that the presence of a magnetic field on large scales ensures a rapid rise of the velocity field on large scales. On the other hand, magnetic field decay on large scales occurs at slow rates.

The structure of our paper is as follows. In Sec. II, we briefly describe magnetic field generation during inflation. In Sec. III, we discuss the phenomenological coupling of the magnetic field to the turbulent plasma. In Sec. IV, we present our numerical simulation results. We discuss our results and conclude in Sec. V.

II. INFLATION-GENERATED MAGNETIC FIELD

A. Nonhelical magnetic field

Any field included in the Lagrangian density during inflation will be produced by quantum-mechanical fluctuations. These fluctuations are then stretched by the cosmological expansion, leaving the Hubble radius during inflation and reentering it at much later times.

Adding the standard Abelian vector field Lagrangian density $F_{\mu\nu}F^{\mu\nu}/\hat{e}^2$ (where $\hat{e}$ is the vector potential coupling constant) to the usual general relativity and scalar inflaton field Lagrangian density results in electric and magnetic fields being generated during inflation. Of course, these are not the usual low-energy electric and magnetic fields; rather, at the very least, they are hypercharge electric and magnetic fields. During inflation, the conductivity vanishes, but particle creation at reheating quickly turns the Universe into a very good conductor at the end of inflation. This short circuits the electric field but does not affect the large-scale magnetic field. For a close to de Sitter exponentially expanding epoch of inflation, on a

scale of a thousandth of a Hubble radius now (i.e., a few Mpc now), the rms magnetic field strength now is of order 10^{-59} G and very insignificant [11]. In this case, the power spectrum of the magnetic field is $|B(k)|^2 \propto k/a^4$, where k is the coordinate wave number, and the evolution with scale factor a is as expected from flux conservation. This tiny value is a consequence of the conformal invariance of the Abelian vector field Lagrangian density and the background spacetime. To generate a large enough magnetic field requires using a model in which conformal invariance is broken [10–12].

A simple way to break conformal invariance is to couple the inflaton scalar field ϕ to the Abelian vector field through a dilatonlike coupling, generalizing the Maxwell Lagrangian density to $e^{\alpha\phi}F_{\mu\nu}F^{\mu\nu}/\hat{e}^2$ (α is a parameter, and the exponential form of the dilationlike coupling was chosen for simplicity) [11,12]. At the end of inflation, during reheating, ϕ freezes at its vacuum expectation value and the usual Abelian vector field Lagrangian density is recovered. During inflation, however, the model behaves as though it has a varying Abelian vector field coupling constant. This modifies the scale factor and wave number dependence of the generated magnetic field. For power-law inflation [29], power is shifted to the infrared, and the magnetic field energy density redshifts slower than the usual uncoupled Abelian vector field case.

Depending on the value of α, this can result in a large enough seed magnetic field to explain the observed galactic magnetic fields. The case of greatest interest is near the limit of de Sitter exponential expansion inflation, which results in a close to scale-invariant Harrison-Peebles-Yu-Zeldovich spectrum of energy density perturbations (consistent with the observational indications; see, e.g., Ref. [30]) with a current epoch magnetic field scale-invariant power spectrum $|B(k)|^2 \propto k^{-3}/a^4$, or $\langle B^2(r)\rangle^{1/2} \propto r$, and rms amplitude of order a few nG on a scale of a thousandth of a Hubble radius [11,12]. These computations have been carefully checked, confirmed, and extended [31]. This is an observationally viable model.

In this model, there are regions in model parameter space where the vector field fluctuations during inflation are large enough to invalidate the linear perturbation assumption, but this does not occur in the region of parameter space where a strong-enough current-epoch large-scale magnetic field is generated [11,12,32,33]. That is, backreaction is not a significant issue for this classically consistent model. While the Abelian vector field coupling becomes large during inflation, this is not important for the phenomenological, effective classical model [1,11,12,32,34]. Instead, much like the case of the "standard" ΛCDM cosmological model, it is of great interest to try to find a more fundamental, quantum-mechanically consistent, model which can give rise to this classical, observationally successful, inflationary magnetogenesis model.

An extension of this model, with two scalar fields instead of one, is also viable [35]. Here, in addition to the usual scalar inflaton field, a new scalar field, coupled as a dilaton to the Abelian vector field, is introduced. Alternatively, as discussed next, the second field is taken to be a pseudoscalar, coupling like an axion to the Abelian vector field. For other inflationary magnetogenesis variants, see Ref. [36].

B. Helical magnetic field

The inverse cascade scenario, a much discussed magnetic field amplification mechanism, requires nonzero magnetic helicity, if it is to be able to transfer magnetic power from small scales to large scales and so amplify the large-scale magnetic field [37]. It is therefore of interest to consider inflationary magnetogenesis models which can also generate magnetic helicity.

In a Friedmann-Lemaître-Robertson-Walker cosmological model, magnetic helicity is [38]

$$H_B(t) = \int d^3x \mathbf{A}\cdot\nabla\times\mathbf{A}, \tag{1}$$

where the vector potential $\mathbf{A}$ is related to the magnetic field through $a^2\mathbf{B} = \nabla\times\mathbf{A}$. Magnetic helicity is usually associated with a nontrivial configuration of the magnetic field where the magnetic flux tubes are twisted and/or linked [26]. Magnetic helicity resembles a Chern-Simons term, for its time variation is given by $H_B(t_2) - H_B(t_1) = \frac{1}{4}\int_{t_1}^{t_2} d^4x F_{\mu\nu}\tilde{F}^{\mu\nu}$ [38], where $\tilde{F}^{\mu\nu}$ is the vector field strength tensor dual. This similarity is strengthened by the fact that a helical magnetic field may be identified as the projection of a non-Abelian gauge field configuration carrying a nonvanishing Chern-Simons number [39], and that the magnetic helicity coincides with this winding number.

Moreover, helical magnetic fields possess a number asymmetry between left-handed and right-handed Abelian vector field helicity states [38]. To see this, it is useful to go to Fourier space and introduce the orthonormal helicity basis $\{\mathbf{e}_+, \mathbf{e}_-, \mathbf{e}_3\}$, with $\mathbf{e}_\pm = (\mathbf{e}_1 \pm i\mathbf{e}_2)/\sqrt{2}$ and $\mathbf{e}_3 = \mathbf{k}/k$, such that $\{\mathbf{e}_1, \mathbf{e}_2, \mathbf{e}_3\}$ form a right-handed orthonormal basis. Decomposing the magnetic field in polarization states as $\mathbf{B}(\mathbf{k}) = B_+\mathbf{e}_+ + B_-\mathbf{e}_-$, the magnetic helicity reads

$$H_B(t) = \frac{a^4}{2\pi^2}\int dk k(|B_+|^2 - |B_-|^2). \tag{2}$$

It is clear, accordingly, that a helical magnetic field possesses a nonzero difference between the number of left- and right-handed Abelian vector potential polarization states.

After reheating, the Universe is a good conductor, and so if a helical magnetic field is created during inflation, its magnetic helicity survives to the present. Since magnetic helicity is odd under discrete P and CP transformations,

a cosmological helical magnetic field would be a signature of macroscopic P and CP violation.

Models for generating helical magnetic fields in the early Universe exist in the literature [10,39–44]. In order to generate a helical magnetic field during inflation, one can add an interaction term of the form $I(\phi)F_{\mu\nu}\tilde{F}^{\mu\nu}$ to the Abelian vector potential Lagrangian density. Here, $I(\phi)$ is a pseudoscalar function of some dynamical or background field ϕ.

A coupling $I(\phi) \propto \phi$, between the Abelian vector potential and the axion field ϕ was studied in Refs. [10,40,41], while in Ref. [42], the pseudoscalar ϕ was assumed to drive inflation. In these cases, because of the extra derivative compared to the $e^{\alpha\phi}F_{\mu\nu}F^{\mu\nu}/\hat{e}^2$ term, magnetic power is concentrated on smaller scales, with insignificant magnetic power on cosmological scales of interest.

In Ref. [43], to produce larger-scale magnetic field power, the function I was taken to be a time-dependent function peaked at long wavelengths (this particular coupling to the Abelian vector potential could be realized by a tachyonic massive pseudoscalar field or a massless pseudoscalar field nonminimally coupled to gravity). It was shown that, depending on the strength of the coupling, a maximally helical field with a scale-invariant spectrum, $|B(k)|^2 \propto k^{-3}$, could be produced as an excitation of the vacuum during inflation. Although it can be quite large, large enough to act as a seed for the magnetic fields we observe today in galaxies and galaxy clusters, as before, its backreaction on the development of inflation is completely negligible.

III. COUPLING OF MAGNETIC FIELD AND TURBULENT MOTIONS

Because of conformal invariance, the usual flat spacetime relativistic MHD equations are identical to the MHD equations in an expanding Universe with zero spatial curvature when physical quantities are replaced by their comoving counterparts and conformal time η is used in place of physical time [45]. Based on this fact, we perform direct numerical simulations of MHD turbulence in an expanding Universe using the usual flat spacetime MHD equations with a relativistic equation of state. Note that our simulations are based on the relativistic equations even when studying evolution of turbulence with nonrelativistic bulk velocities.

Let us briefly describe the primordial magnetic field coupling to the fluid. As noted above, the typical characteristic length scale of this coupling is the phase transition bubble size, $\lambda_0 = \gamma\lambda_H$, where $\gamma < 1$ is a parameter connected with the number of bubbles, N, within a Hubble radius, i.e., $\gamma^{-1} \propto N^3$, and the Hubble radius

$$\lambda_H = 5.8 \times 10^{-10}\ \mathrm{Mpc}\left(\frac{100\ \mathrm{GeV}}{T_\star}\right)\left(\frac{100}{g_\star}\right)^{1/6}. \quad (3)$$

As we noted above, we will consider both electroweak and QCD phase transitions. The phase transitions are characterized by different maximal correlation lengths due to the difference in the γ parameter (which is equal to 0.01 and 0.15 for electroweak and QCD phase transitions, respectively) and in the Hubble radius; see Eq. (3) (which is equal to 0.006 μpc and 5.5 pc for electroweak and QCD phase transitions, respectively). As we noted above, the initial value of the Alfvén velocity depends weakly on $g_\star(v_A \propto g_\star^{-1/6})$, which also makes a difference between the electroweak and QCD phase transitions of the order of unity (1.37), which we discard. The conductivity of the Universe is high enough during the phase transitions: of course, the physical characteristics of the plasma (such as viscosity and conductivity) depend on temperature and vary from 100 GeV (electroweak phase transition) to 0.15 eV (QCD phase transition). On the other hand, in our simulations, we assume that, for the goal of our study, the main difference between the electroweak and QCD phase transitions consists only in a difference of the initial correlation length. Our assumption can be justified as follows: (i) the forcing amplitude at the initial moment weakly depends on the relativistic degrees of freedom, $\propto g_\star^{-1/6}$; (ii) the physical conditions of the Universe are different, but new simulations for a wide range of the Prandtl numbers show that the growth of the correlation length does not depend on the value of the Reynolds number, as long as it is large enough [46].

We consider two types of forcings, irrotational and vortical, and for both, we assume that the forcing scale coincides with the bubble size, λ_0. The corresponding wave number is $k_0 = 2\pi/\lambda_0$. Energy is being dissipated both viscously (characterized by the viscosity ν) and ohmically (characterized by the magnetic diffusivity λ, which is inversely proportional to the conductivity). Throughout this work, we assume that the magnetic Prandtl number is $\nu/\lambda = 1$. The smaller the value of ν, the more extended the turbulent cascade, and the larger the minimal mesh resolution required. For all runs presented here, we use 512^3 mesh points. The largest value of the Reynolds number based on the wave number k_0, $\mathrm{Re} \equiv u_{\mathrm{rms}}/\nu k_0$, is around 200 in all cases (here, u_{rms} is the rms velocity).

There are many MHD simulations which use vortical forcing [23] but fewer which use irrotational forcing [47]. However, we are unaware of any simulation with an initial scale-invariant magnetic field spectrum, $|B(k)|^2 \propto k^{-3}$, of appreciable strength.[3] We generate the corresponding magnetic vector potential for such a field in Fourier space using

[3]We require that the magnetic field satisfies the upper limits from the current CMB and large-scale structure observations, [13] (which automatically satisfy the big bang nucleosynthesis limits), so to be order of few nG. Such a magnetic field can be generated during inflation [11]. For helical magnetic fields, we assume that they are of maximal helicity [43].

modes with random phases and suitable amplitudes, as was done in Ref. [48] for the initial velocity field using the PENCIL CODE [49], which is also used here. We present magnetic and kinetic energy spectra normalized such that $\int E_{\rm M}(k)dk = \langle \mathbf{B}^2 \rangle/2$ and $\int E_{\rm K}(k)dk = \langle \mathbf{u}^2 \rangle/2$, respectively.

In all cases, we keep the forcing amplitude at a fixed level such that the resulting rms velocity is around $0.1c_{\rm s}$, where the constant $c_{\rm s}$ is the isothermal sound speed. The rms value of initial magnetic field strength, $B^{(0)}_{\rm rms}$, is chosen such that $B^{(0)}_{\rm rms}/c_{\rm s}$ is between 0.05 and 0.09.

In the following, we describe the types of forcing applied to the system.

A. Irrotational (potential) forcing

We consider two types of irrotational forcings. In both cases, the forcing function is written as $\boldsymbol{f}(\boldsymbol{x}, t) = \nabla\phi$, where $\phi(\boldsymbol{x}, t)$ is a random scalar function. In the first case, we model irrotational forcing in the form of spherical expansion waves which reflect the dynamics of phase transition bubbles. The forcing and some results for cases with no or weak magnetic fields are described in Refs. [47,50]. The nondimensional radius of the expansion waves is $k_1 R = 0.133$, corresponding to a nominal forcing wave number $k_0/k_1 = 15$. Here, $k_1 = 2\pi/L$ is the minimal wave number in our computational cube of size L^3. In the second case, we use random plane waves with a wave number $k_0/k_1 = 30$.

B. Vortical forcing

Vortical forcing is accomplished by generating a random vector potential $\boldsymbol{\psi}$ such that $\boldsymbol{f} = \nabla \times \boldsymbol{\psi}$. Normally, $\boldsymbol{\psi}$ is nonhelical, but in some cases, we have arranged $\boldsymbol{\psi}$ such that it consists of positively polarized waves [23]. Like in the second case with potential forcing, the forcing wave number is here chosen to be $k_0/k_1 = 30$.

IV. RESULTS

A. Blob-like forcing

Bloblike irrotational [47] and plane wave [51] forcings have been used in the past to investigate the production of vorticity through the viscous force, or through the interaction of irrotationally forced flow with global rotation or shear with an isothermal equation of state, or through the baroclinic term with the more general perfect gas equation of state [50]. In the present case, again using an isothermal gas, the Lorentz force associated with the initial magnetic field also produces vorticity [52].

In all cases investigated here, the magnetic energy density decays, so there is either no dynamo action, or the initial magnetic field is still too strong for dynamo action to occur because of excessive backreaction on the flow via the Lorentz force. As the magnetic field decays, the level of vorticity also decreases. In fact, at the end of the simulation,

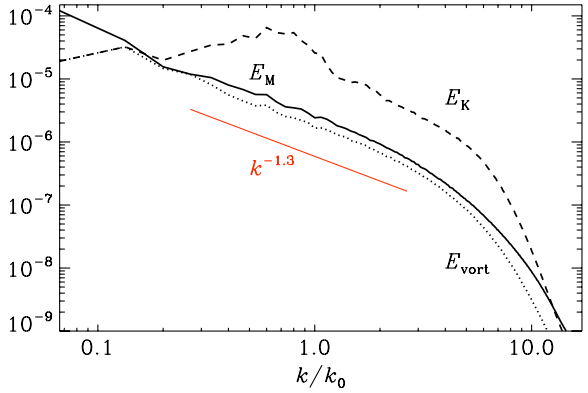

FIG. 1 (color online). Spectra of magnetic and kinetic energy as well as the kinetic energy of the vortical component at the end of the run for vortical bloblike forcing. Re ≈ 250 and $B^{(0)}_{\rm rms}/c_{\rm s}0.05$.

the spectrum of the vortical part of the kinetic energy follows closely that of the magnetic energy; see Fig. 1. The rms vorticity turns out to be approximately proportional to the magnetic energy density. Quantitatively, we find $\omega_{\rm rms}/u_{\rm rms}k_0 \approx 0.1(\mathcal{E}_{\rm M}/\mathcal{E}_{\rm K})^{0.85}$; see Fig. 2. Here, $\omega_{\rm rms}$ is the rms vorticity, and $\mathcal{E}_{\rm M}$ and $\mathcal{E}_{\rm K}$ are the magnetic and kinetic energy densities. (We note that the exponent 0.85 is probably not robust; in another simulation, we have found a somewhat larger exponent ≈ 1.2, for example.)

During the rising phase of the kinetic energy, the kinetic energy spectrum is approximately proportional to k^2. At small scales, we have an approximate k^{-2} spectrum, in agreement with earlier studies [47,50]. Here, the spectral magnetic energy exceeds the total spectral kinetic energy, and the vortical part of the kinetic energy spectrum is only slightly below that of the total kinetic energy spectrum.

B. Monochromatic vortical forcing

Next, we consider the case of monochromatic vortical forcing. In the simulations presented here, the spectrum of kinetic energy is below that of the magnetic energy, but it still shows a k^2 behavior at small wave numbers and intermediate times. At earlier times, the spectrum is closer

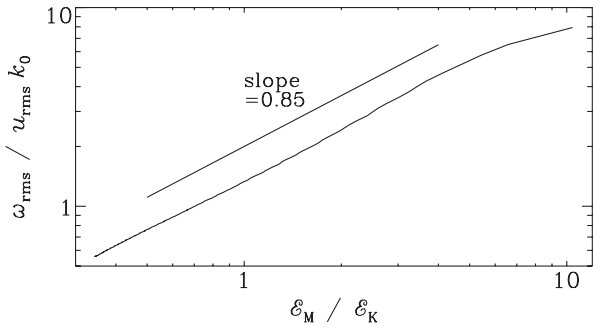

FIG. 2. Dependence of normalized rms vorticity on normalized magnetic energy density during the decay for the run shown in Fig. 1 for Re ≈ 250.

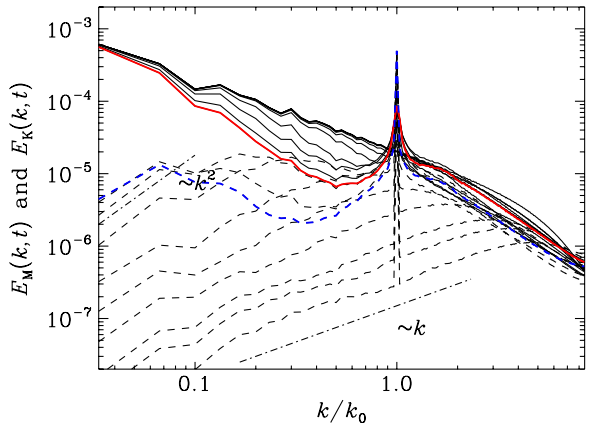

FIG. 3 (color online). Magnetic (solid lines) and kinetic (dashed lines) energy spectra in regular time intervals. Re $\approx$ 170. The magnetic and kinetic spectra at the last time are additionally marked in red and blue, respectively. Re $\approx$ 180 and $B_{\rm rms}^{(0)}/c_{\rm s}0.09$.

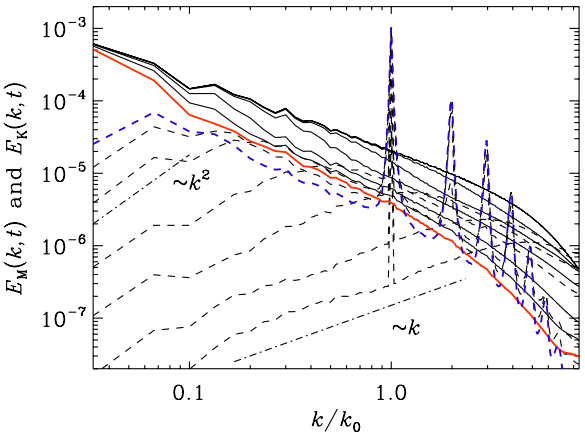

FIG. 5 (color online). Similar to Fig. 3, but for potential forcing with plane waves. Re $\approx$ 220 and $B_{\rm rms}^{(0)}/c_{\rm s}0.09$.

to a linearly increasing one; see Fig. 3. At intermediate times, there is a characteristic decline of magnetic energy at intermediate wave numbers ($k/k_0 \approx 0.3$), which then leads to a similar decline of the kinetic energy at these wave numbers.

Visualizations of the B_x component of the magnetic field and of the logarithmic density, $\ln\rho$, are given in Fig. 4 for early and late times. The initial k^{-1} magnetic energy spectrum manifests itself in the form of large random patches which also give an imprint on $\ln\rho$. However, as the forcing proceeds, small-scale structures of scale λ_0 become visible in $\ln\rho$ as well as in B_x. This is quite different in the case of irrotational forcing, of which we describe the results from a plane-wave forcing formulation next.

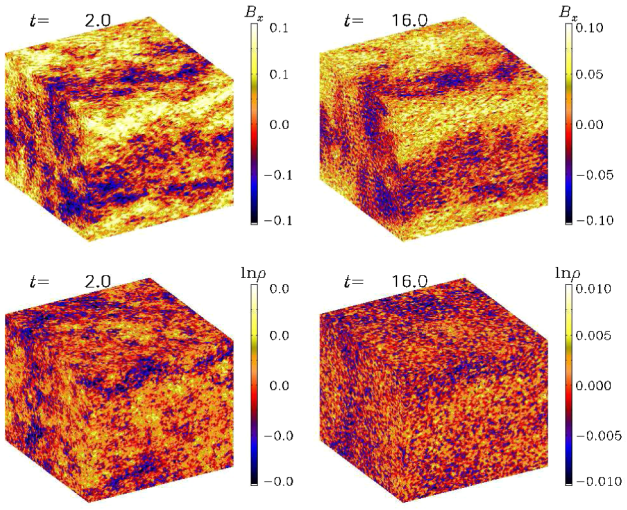

FIG. 4 (color online). Visualization of the B_x component and $\ln\rho$ for the run shown in Fig. 3. Note that at late times, the small-scale velocity variations cause a corresponding imprint on the magnetic field structure. $u_{\rm rms}/c_{\rm s} = 0.05$ and Re $\approx$ 180.

C. Irrotational plane-wave forcing

The irrotational forcing considered in Sec. IV A is more realistic for applications to phase transition bubbles than is plane-wave forcing, but to ease the comparison with the vortical forcing considered in Sec. IV B, we now consider the case of plane-wave irrotational forcing. In this case, the spectra show initially the same behavior as in the vortical case. Even at late times, there are similarities, except that the magnetic and kinetic energy spectra now lack the characteristic decline which was visible in the vortical case at $k/k_0 \approx 0.3$; see Fig. 5. This is because the irrotational part of the flow does not interact directly and sufficiently strongly with the magnetic field. This is also clear from visualizations shown in Fig. 6 which demonstrate that the small-scale structures of scale λ_0 leave no imprint on the magnetic field.

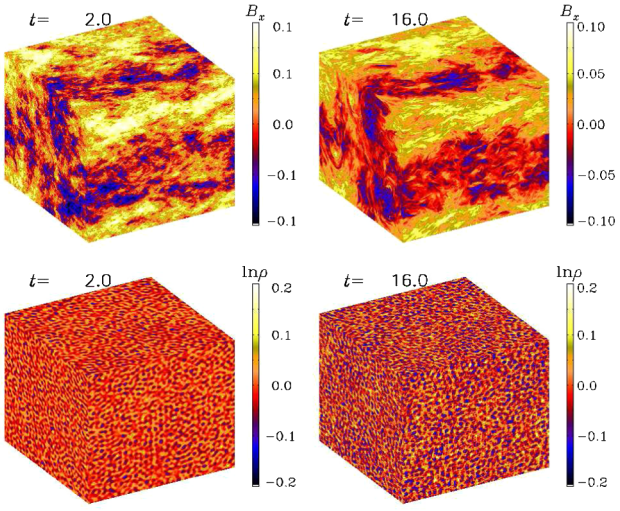

FIG. 6 (color online). Visualization of the B_x component and $\ln\rho$ for the run shown in Fig. 5. Potential forcing (plane waves). Note that at late times, the small-scale velocity field has hardly any impact on the magnetic field. $u_{\rm rms}/c_{\rm s} = 0.07$ and Re $\approx$ 220.

In Fig. 7, we compare spectra of magnetic and kinetic energy at early and late times for vortical and irrotational plane-wave forcing. At the early time, the spectra are independent of the nature of the forcing, so we show here, in the upper panel, only the vortical case at $t = 0.5/c_s k_1$. At a later time ($t = 10/c_s k_1$), the kinetic and magnetic energy spectra show a decline at intermediate wave numbers for the vortical case (see middle panel), as already discussed above. The result for the helical case is virtually indistinguishable. This is because magnetic energy tends to drive the transfer of magnetic energy to larger scales, but the spectral magnetic energy at those scales is now already rather strong. In the irrotational case (see bottom panel), the decline at $k/k_0 \approx 0.3$ does not exist. This is because here vorticity is small, and only this vortical part of the flow interacts with the magnetic field and leads then to turbulent diffusion of the field through mixing.

D. Comparison with helical forcing

As we have seen in Fig. 7, there is virtually no difference between vortical forcings with and without helicity. This is probably related to the fact that there was not enough time for the helical forcing to affect magnetic and velocity fields at scales larger than the injection scale. This can be seen from Fig. 8, where we compare cases with helical and nonhelical forcings for magnetic and kinetic helicity spectra, $H_M(k)$ and $H_K(k)$, respectively. These spectra are normalized such that $\int H_M(k)dk = \langle \mathbf{A} \cdot \mathbf{B} \rangle$ and $\int H_K(k)dk = \langle \boldsymbol{\omega} \cdot \mathbf{u} \rangle$, where $\boldsymbol{\omega} = \nabla \times \mathbf{u}$ is the vorticity. These spectra are shown together with their respective magnetic and kinetic energy spectra, $E_M(k)$ and $E_K(k)$, respectively. They satisfy the realizability conditions, $E_M \geq |\frac{1}{2} k H_M|$ and $E_K \geq |\frac{1}{2} H_K/k|$, respectively [53]. (Note that the definitions of H_M and H_K relative to those of E_M and E_K differ from each other by a k^2 factor, which explains the slight difference from of their respective realizability conditions.)

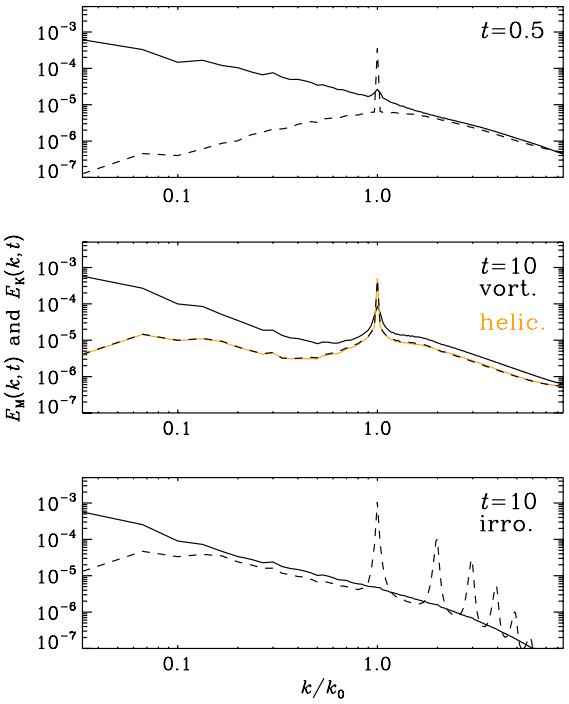

FIG. 7 (color online). Comparison of magnetic (solid lines) and kinetic (dashed lines) energy spectra at early and late times for vortical and irrotational plane-wave forcing. The vortical case with helicity is shown in orange, and nearly coincides with the nonhelical case (dashed). At early times, the spectra are independent of the nature of the forcing.

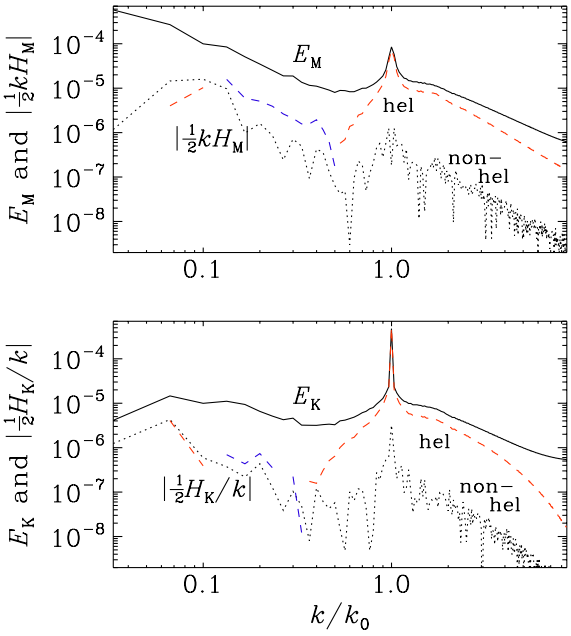

FIG. 8 (color online). Comparison of normalized magnetic (upper panel) and kinetic (lower panel) helicity spectra for cases with helical (dashed) and nonhelical (dotted) forcings. In the case with helical forcing (dashed lines), red/blue segments indicate positive/negative values of H_M and H_K. For comparison, we also show magnetic and kinetic energy spectra in the upper and lower panels, respectively.

Figure 8 shows that in the case with helical forcing, where the kinetic helicity is positive, $\frac{1}{2} k H_M(k)$ is also positive and close to $E_M(k)$ for $k \approx k_0$, but about an order of magnitude below it for smaller values of k. This supports the suggestion that helicity effects are too small to modify the energy spectra significantly.

V. CONCLUSION

In this paper, we have studied the evolution of an inflation-generated magnetic field [11] coupled to the fluid during cosmological phase transitions. Our formalism is very general and applies to the electroweak and QCD phase transitions. The difference between these (and other)

phase transitions is encoded in the difference in parameters such as the temperature and the number of relativistic degrees of freedom, parameters which determine the characteristic length scale of the system under consideration (λ_0). We consider different types of forcing and show that at late times, the kinetic energy spectrum depends sensitively on the forcing used.

Our forcing scale is determined by the phase transition bubble size. Within a few turnover times, the kinetic energy spectrum starts to rise on large scales, generating large-scale turbulent motions in the fluid. Even a rapid phase transition generates turbulence, which will slowly decay on large scales. Phase transition-generated MHD turbulence might be relevant for cosmological magnetogenesis [3]. Phase transition turbulence can also generate a gravitational wave signal which is potentially detectable [54].

In contrast to previous studies, the inflation-generated magnetic field is not frozen into the cosmic plasma. The forcing which we considered here is limited by the duration of the phase transition. After the forcing source stops acting, both magnetic and kinetic energies start to decay freely. The configuration of the magnetic field at large scales (outside the phase transition Hubble radius) is almost unchanged. At intermediate scales corresponding to the phase transition bubble size, there is a slight suppression due to energy conversion into kinetic energy. The induced turbulent motions are causal, so the spectral shape at large scales is given by a white noise spectrum $E_K(k) \propto k^2$ [55]; the vorticity energy density spectrum will be steeper (k^4) due to the additional requirement of causality [56]. The presence of magnetic helicity does not significantly change the forcing stage. On the other hand, the scaling laws in the decay stage are strongly affected by the presence of magnetic helicity. The duration of the decay stage is much longer than the forcing stage. During this stage, the correlation length of the velocity increases with a corresponding decay of the total energy density. The magnetic field on super-Hubble-radius scales is decoupled from the fluid which, in turn, stays almost unaffected.

The main results of our study are: (i) inflation-generated magnetic fields are not significantly modified on large scales by their coupling to the plasma during a cosmological phase transition; (ii) the coupling of the magnetic field with the phase transition fluid leads to deviations of the magnetic field spectrum from the initial scale-invariant shape on intermediate scales; and (iii) there is the possibility of having large-scale correlated turbulent motions in the early Universe which, eventually, could affect the development of large-scale structure formation at late times, and in particular cluster physics [57].

ACKNOWLEDGMENTS

We appreciate useful discussions with C. Caprini, K. Jedamzik, A. Kosowsky, A. Kravtsov, A. Neronov, and D. Semikoz. Computing resources have been provided by the Swedish National Allocations Committee at the Center for Parallel Computers at the Royal Institute of Technology in Stockholm and and by the Carnegie Mellon University supercomputer center. We acknowledge partial support from DOE Grant No. DEFG030-99EP41093, Swiss National Science Foundation SCOPES Grant No. 128040, NSF Grants No. AST-1109180 and No. AST-1109275, NASA Astrophysics Theory Program Grant No. NNXlOAC85G, European Research Council AstroDyn Research Project 227952, and Swedish Research Council Grant No. 621-2007-4064. T. K. acknowledges the ICTP associate membership program. A. B. and A. T. acknowledge the hospitality of the McWilliams Center for Cosmology where part of this work was performed.

[1] K. Subramanian, Astron. Nachr. **331**, 110 (2010).
[2] A. Kandus, K. E. Kunze, and C. G. Tsagas, Phys. Rep. **505**, 1 (2011).
[3] L. M. Widrow, D. Ryu, D. R. G. Schleicher, K. Subramanian, C. G. Tsagas, and R. A. Treumann, Space Sci. Rev. **166**, 37 (2012).
[4] D. G. Yamazaki, T. Kajino, G. J. Mathews, and K. Ichiki, Phys. Rep. **517**, 141 (2012).
[5] T. Kahniashvili, A. Tevzadze, S. Sethi, K. Pandey, and B. Ratra, Phys. Rev. D **82**, 083005 (2010).
[6] A. Neronov and I. Vovk, Science **328**, 73 (2010); F. Tavecchio, G. Ghisellini, L. Foschini, G. Bonnoli, G. Ghirlanda, and P. Coppi, Mon. Not. R. Astron. Soc. **406**, L70 (2010); S. Ando and A. Kusenko, Astrophys. J. **722**, L39 (2010); A. Neronov, D. V. Semikoz, P. G. Tinyakov, and I. I. Tkachev, Astron. Astrophys. **526**, A90 (2011); F. Tavecchio, G. Ghisellini, G. Bonnoli, and L. Foschini, Mon. Not. R. Astron. Soc. **414**, 3566 (2011); K. Dolag, M. Kachelriess, S. Ostapchenko, and R. Tomas, Astrophys. J. **727**, L4 (2011); W. Essey, S. Ando, and A. Kusenko, Astropart. Phys. **35**, 135 (2011); A. M. Taylor, I. Vovk, and A. Neronov, Astron. Astrophys. **529**, A144 (2011); H. Huan, T. Weisgarber, T. Arlen, and S. P. Wakely, Astrophys. J. Lett. **735**, L28 (2011); I. Vovk, A. M. Taylor, D. Semikoz, and A. Neronov, Astrophys. J. Lett. **747**, L14 (2012).
[7] C. D. Dermer, M. Cavadini, S. Razzaque, J. D. Finke, J. Chiang, and B. Lott, Astrophys. J. **733**, L21 (2011); K. Takahashi, M. Mori, K. Ichiki, and S. Inoue, Astrophys. J. **744**, L7 (2012).

[8] A. E. Broderick, P. Chang, and C. Pfrommer, Astrophys. J. **752**, 22 (2012).

[9] W. Fischler, B. Ratra, and L. Susskind, Nucl. Phys. **B259**, 730 (1985).

[10] M. S. Turner and L. M. Widrow, Phys. Rev. D **37**, 2743 (1988).

[11] B. Ratra, Astrophys. J. **391**, L1 (1992).

[12] B. Ratra, Caltech preprint Report No. GRP-287/CALT-68-1751, 1991 available at http://www.phys.ksu.edu/personal/ratra/.

[13] T. Kahniashvili and B. Ratra, Phys. Rev. D **75**, 023002 (2007); J. R. Kristiansen and P. G. Ferreira, Phys. Rev. D **77**, 123004 (2008); D. Paoletti, F. Finelli, and F. Paci, Mon. Not. R. Astron. Soc. **396**, 523 (2009); K. Ichiki, K. Takahashi, and N. Sugiyama, Phys. Rev. D **85**, 043009 (2012); K. E. Kunze, Phys. Rev. D **85**, 083004 (2012); D. G. Yamazaki, K. Ichiki, T. Kajino, and G. J. Mathews, Adv. Astron. **2010**, 586590 (2010); J. R. Shaw and A. Lewis, Phys. Rev. D **86**, 043510 (2012).

[14] G. Chen, P. Mukherjee, T. Kahniashvili, B. Ratra, and Y. Wang, Astrophys. J. **611**, 655 (2004); I. Brown and R. Crittenden, Phys. Rev. D **72**, 063002 (2005); M. Demianski and A. G. Doroshkevich, Phys. Rev. D **75**, 123517 (2007); A. Bernui and W. S. Hipolito-Ricaldi, Mon. Not. R. Astron. Soc. **389**, 1453 (2008); T. Kahniashvili, G. Lavrelashvili, and B. Ratra, Phys. Rev. D **78**, 063012 (2008); P. K. Samal, R. Saha, P. Jain, and J. P. Ralston, Mon. Not. R. Astron. Soc. **396**, 511 (2009); P. Trivedi, T. R. Seshadri, and K. Subramanian, Phys. Rev. Lett. **108**, 231301 (2012); C. Bonvin, C. Caprini, and R. Durrer, Phys. Rev. D **86**, 023519 (2012), and references therein.

[15] M. Kawasaki and M. Kusakabe, Phys. Rev. D **86**, 063003 (2012), and references therein.

[16] M. Giovannini and K. E. Kunze, Phys. Rev. D **78**, 023010 (2008); T. Kahniashvili, Y. Maravin, and A. Kosowsky, Phys. Rev. D **80**, 023009 (2009); L. Pogosian, A. P. S. Yadav, Y.-F. Ng, and T. Vachaspati, Phys. Rev. D **84**, 043530 (2011), and references therein.

[17] D. V. Deriagin, D. Iu. Grigor'ev, V. A. Rubakov, and M. V. Sazhin, Mon. Not. R. Astron. Soc. **229**, 357 (1987); C. Caprini and R. Durrer, Phys. Rev. D **65**, 023517 (2001); T. Kahniashvili, A. G. Tevzadze, and B. Ratra, Astrophys. J. **726**, 78 (2011).

[18] S. Wang, Phys. Rev. D **81**, 023002 (2010).

[19] M. Christensson, M. Hindmarsh, and A. Brandenburg, Phys. Rev. E **64**, 056405 (2001).

[20] L. Campanelli, Phys. Rev. D **70**, 083009 (2004).

[21] R. Banerjee and K. Jedamzik, Phys. Rev. Lett. **91**, 251301 (2003); Phys. Rev. D **70**, 123003 (2004).

[22] L. Campanelli, Phys. Rev. Lett. **98**, 251302 (2007).

[23] N. E. Haugen, A. Brandenburg, and W. Dobler, Phys. Rev. E **70**, 016308 (2004).

[24] C. Caprini, R. Durrer, and E. Fenu, J. Cosmol. Astropart. Phys. 11 (2009) 001.

[25] M. Christensson, M. Hindmarsh, and A. Brandenburg, Astron. Nachr. **326**, 393 (2005).

[26] D. Biskamp, *Magnetohydrodynamic Turbulence* (Cambridge University, Cambridge, England, 2003).

[27] T. Kahniashvili, A. Brandenburg, A. G. Tevzadze, and B. Ratra, Phys. Rev. D **81**, 123002 (2010).

[28] A. Kosowsky and M. S. Turner, Phys. Rev. D **47**, 4372 (1993).

[29] B. Ratra, Phys. Rev. D **40**, 3939 (1989); **45**, 1913 (1992).

[30] B. Ratra and M. S. Vogeley, Publ. Astron. Soc. Pac. **120**, 235 (2008).

[31] K. Bamba and J. Yokoyama, Phys. Rev. D **69**, 043507 (2004); J. Martin and J. Yokoyama, J. Cosmol. Astropart. Phys. 01 (2008) 025.

[32] V. Demozzi, V. Mukhanov, and H. Rubinstein, J. Cosmol. Astropart. Phys. 08 (2009) 025.

[33] S. Kanno, J. Soda, and M.-a. Watanabe, J. Cosmol. Astropart. Phys. 12 (2009) 009; R. Enami, H. Firouzjahi, and M. S. Movahed, Phys. Rev. D **81**, 083526 (2010); V. Demozzi and C. Ringeval, J. Cosmol. Astropart. Phys. 05 (2012) 009; L. Motta and R. R. Caldwell, Phys. Rev. D **85**, 103532 (2012).

[34] R. R. Caldwell, L. Motta, and M. Kamionkowski, Phys. Rev. D **84**, 123525 (2011); N. Barnaby, R. Namba, and M. Peloso, Phys. Rev. D **85**, 123523 (2012).

[35] D. Lemoine and M. Lemoine, Phys. Rev. D **52**, 1955 (1995); M. Gasperini, M. Giovannini, and G. Veneziano, Phys. Rev. Lett. **75**, 3796 (1995); K. Bamba and J. Yokoyama, Phys. Rev. D **69**, 043507 (2004).

[36] G. Lambiase, S. Mohanty, and G. Scarpetta, J. Cosmol. Astropart. Phys. 07 (2008) 019; L. Campanelli, P. Cea, G. L. Fogli, and L. Tedesco, Phys. Rev. D **77**, 043001 (2008); K. Bamba, N. Ohta, and S. Tsujikawa, Phys. Rev. D **78**, 043524 (2008); L. Campanelli and P. Cea, Phys. Lett. B **675**, 155 (2009); K. E. Kunze, Phys. Rev. D **81**, 043526 (2010), and references therein.

[37] A. Brandenburg, D. Sokoloff, and K. Subramanian, Space Sci. Rev. **169**, 123 (2012).

[38] L. Campanelli and M. Giannotti, Phys. Rev. D **72**, 123001 (2005).

[39] R. Jackiw and S.-Y. Pi, Phys. Rev. D **61**, 105015 (2000).

[40] W. D. Garretson, G. B. Field, and S. M. Carroll, Phys. Rev. D **46**, 5346 (1992).

[41] G. B. Field and S. M. Carroll, Phys. Rev. D **62**, 103008 (2000).

[42] T. Prokopec, arXiv:astro-ph/0106247.

[43] L. Campanelli, Int. J. Mod. Phys. D **18**, 1395 (2009).

[44] J. M. Cornwall, Phys. Rev. D **56**, 6146 (1997); M. Giovannini, Phys. Rev. D **61**, 063004 (2000); T. Vachaspati, Phys. Rev. Lett. **87**, 251302 (2001); D. S. Lee, W. Lee, and K. W. Ng, Phys. Lett. B **542**, 1 (2002); M. Laine, J. High Energy Phys. 10 (2005) 056; M. M. Anber and L. Sorbo, J. Cosmol. Astropart. Phys. 10 (2006) 018; V. B. Semikoz and D. D. Sokoloff, Int. J. Mod. Phys. D **14**, 1839 (2005); A. Diaz-Gil, J. Garcia-Bellido, M. Garcia Perez, and A. Gonzalez-Arroyo, Phys. Rev. Lett. **100**, 241301 (2008); C. J. Copi, F. Ferrer, T. Vachaspati, and A. Achucarro, Phys. Rev. Lett. **101**, 171302 (2008); L. Campanelli, P. Cea, and G. L. Fogli, Phys. Lett. B **680**, 125 (2009); R. Durrer, L. Hollenstein, and R. K. Jain, J. Cosmol. Astropart. Phys. 03 (2011) 037.

[45] A. Brandenburg, K. Enqvist, and P. Olesen, Phys. Rev. D **54**, 1291 (1996).

[46] A. Brandenburg, T. Kahniashvili, and A. Tevzadze (work in progress).

[47] A. J. Mee and A. Brandenburg, Mon. Not. R. Astron. Soc. **370**, 415 (2006).
[48] T. A. Yousef, N. E. L. Haugen, and A. Brandenburg, Phys. Rev. E **69**, 056303 (2004).
[49] http://pencil-code.googlecode.com/
[50] F. Del Sordo and A. Brandenburg, Astron. Astrophys. **528**, A145 (2011).
[51] C. Federrath, G. Chabrier, J. Schober, R. Banerjee, R. Klessen, and D. Schleicher, Phys. Rev. Lett. **107**, 114504 (2011).
[52] F. Dosopoulou, F. Del Sordo, C. G. Tsagas, and A. Brandenburg, Phys. Rev. D **85**, 063514 (2012).
[53] H. K. Moffatt, J. Fluid Mech. **35**, 117 (1969).
[54] P. Binetruy, A. Bohe, C. Caprini, and J.-F. Dufaux, J. Cosmol. Astropart. Phys. 06 (2012) 027.
[55] C. J. Hogan, Phys. Rev. Lett. **51**, 1488 (1983).
[56] R. Durrer and C. Caprini, J. Cosmol. Astropart. Phys. 11 (2003) 010.
[57] A. Kravtsov and S. Borgani, Annu. Rev. Astron. Astrophys. **50**, 353 (2012).